ELSEVIER

Since January 2020 Elsevier has created a COVID-19 resource centre with free information in English and Mandarin on the novel coronavirus COVID-19. The COVID-19 resource centre is hosted on Elsevier Connect, the company's public news and information website.

Elsevier hereby grants permission to make all its COVID-19-related research that is available on the COVID-19 resource centre - including this research content - immediately available in PubMed Central and other publicly funded repositories, such as the WHO COVID database with rights for unrestricted research re-use and analyses in any form or by any means with acknowledgement of the original source. These permissions are granted for free by Elsevier for as long as the COVID-19 resource centre remains active.

King Saud University

Arabian Journal of Chemistry

www.ksu.edu.sa
www.sciencedirect.com

ORIGINAL ARTICLE

In silico screening, SAR and kinetic studies of naturally occurring flavonoids against SARS CoV-2 main protease

Muhammad Imran [a], **Sana Iqbal** [b], **Ajaz Hussain** [b,*], **Jalal Uddin** [c,*],
Mohsin Shahzad [d], **Tanwir Khaliq** [d], **Abdul Razzaq Ahmed** [e], **Laiba Mushtaq** [a],
Muhammad Kashif [f], **Khalid Mahmood** [b]

[a] *Department of Chemistry, Faculty of Science, King Khalid University, P.O. Box 9004, Abha 61413, Saudi Arabia*
[b] *Institute of Chemical Sciences, Bahauddin Zakariya University, Multan 60800, Pakistan*
[c] *Department of Pharmaceutical Chemistry, College of Pharmacy, King Khalid University, P.O. Box 9004, Abha 62529, Saudi Arabia*
[d] *Department of Molecular Biology and Biochemistry, Shaheed Zulfiqar Ali Bhutto Medical University Islamabad, Pakistan*
[e] *Department of Prosthodontics, College of Dentistry, King Khalid University, 62529 Abha, Kingdom of Saudi Arabia*
[f] *Government Emerson College, Bosan Road Multan, 60000, Pakistan*

Abstract The Severe Acute Respiratory Syndrome Coronavirus (SARS-CoV-2) pandemic has become a global challenge based on its replication within the host cells that relies on non-structural proteins, protease (M^{pro}). Flavonoids, an important class of naturally occurring compounds with medicinal importance, are frequently available within fruits and vegetables. Herein, we report the *in silico* studies on naturally occurring flavonoids consisting of molecular docking studies and evaluation of theoretical kinetics. In this study, we prepared a library of nine different classes of naturally occurring flavonoids and screened them on Autodock and Autodockvina. The pharmacokinetic properties of most promising compounds have been predicted through ADMET SAR, inhibition constants, ligand efficiency and ligand fit quality have been worked out theoretically. The results revealed that naturally occurring flavonoids could fit well in the receptor's catalytic pocket, interact with essential amino acid residues and could be useful for future drug candidates through *in vitro* and *in vivo* studies. Moreover, MD simulation studies were conducted for two most promising flavonoids and the protein–ligand complexes were found quite stable. The

---

* Corresponding authors.
E-mail addresses: drajazhussain@bzu.edu.pk (A. Hussain), jalaluddinamin@gmail.com (J. Uddin).
Peer review under responsibility of King Saud University.

Production and hosting by Elsevier

selected natural flavonoids are free from any toxic effects and can be consumed as a preventive measure against SARS CoV-2.

1. Introduction

The severe acute respiratory syndrome corona virus-2 (SARS-CoV-2) belongs to the family Coronaviridae and is known to cause respiratory disorders and digestive tract infections (Hui et al., 2020) in both humans and animals. In humans, coronavirus infection caused acute lung injury that changed to ARDS (acute respiratory distress syndrome) and resulted in the COVID-19, a condition associated with person-to-person transmission. Emerging and reemerging new coronavirus strains have become a global challenge for public health concerns and become a global pandemic. Different countries adopt various strategies to treat COVID-19, including social distancing, self-quarantine, and anti-HIV and anti-malarial drugs (Colson et al., 2020, Musarrat et al., 2020). The high rate of recombination and novelty of the 2019n-CoV are major reasons for its abrupt damage and widespread. Hence to combat the COVID-19, the search for new antiviral agents is of great interest rather than vaccine therapy.

The SARS-CoV-2 is an enveloped virus containing a non-segmented single-stranded positive-sense RNA, and the envelope possesses the glycoprotein projections. The genome of n-CoV revealed six open reading frames (OFRs), and the first OFRs encode the two large proteins, polyprotein 1a, and polyprotein 1b (pp1b). These polyproteins being responsible for viral replication and transcription, are processed by Chymotrypsin like Protease (3CL^{pro}) or Main Protease (M^{pro}) and Papain-like Protease into sixteen non-structural proteins (16 nsps). The remaining OFRs encode the four structural proteins, including spike (S), membrane (m), envelope (E), and nucleocapsid (N) proteins (Ziebuhr et al., 2000, Tufan et al., 2020). The spike protein binds to the host cell, namely ACE2 (angiotensin-converting enzyme 2), and leads the entry of SARS-CoV-2 to the host cell (Walls et al., 2020). Precisely speaking, papain-like protease (PL$_{pro}$) and 3-chymotrypsin-like Protease (3CL^{pro}) or M^{pro} is indispensable for CoV replication and also play a role in the inhibition of immune responses (Báez-Santos et al., 2015, Amin et al., 2020). Thus, any interruption in the main Protease is of prime significance for blocking viral replication. The proteases have very little similarity with human proteases and make the drugs less toxic to humans (Anand et al., 2002). Hence targeting the main Protease appears crucial for COVID-19, including SARS (Drosten et al., 2003, Zhong et al., 2003) and MERS-CoV (Zaki et al., 2012) treatment.

The absence of specific therapy for COVID-19 leads to medicinal herbs in several regions of the world. Flavonoids are natural phytochemical compound with several biological activities such as anti-inflammatory, analgesic, antibacterial, antifungal, antiviral, anticarcinogenic, carbonic anhydrase and cholinesterase inhibitory properties (Havsteen, 1983, Pietta, 2000, Imran et al., 2020). Although flavonoids have been reported to have antiviral activity against several types of viruses, the molecular mechanism was rarely known. The

compounds like Kaempferol, Narigenin, Epigenin, and Quercetin show a pharmacophore similar to nelfinavir, a protease inhibitor, effective against HIV (human immunodeficiency virus) (Dabeek and Marra, 2019, Salehi et al., 2019, Yamamoto et al., 2004). ACE2 is a receptor of the coronavirus; thus, compounds that can inhibit the activity of the ACE2 enzyme are also considered helpful in COVID-19 treatment (Zhang et al., 2020, Li et al., 2003). Some citrus flavonoids have been reported to bind the ACE2 enzyme. In most severe COVID-19 patients, a cytokine storm was observed (Huang et al., 2020b). The host immunity's antiviral response involves producing several pro-inflammatory cytokines and activating the T-cells, which are essential for controlling the viral replication, inflammation, and cleaning the cells (Li et al., 2020, Ivashkiv and Donlin, 2014). However, the excessive immune responses lead to cytokine stormcytokine storm formation, known as macrophage activation syndrome (MAS), to further tissue damage (Tufan et al., 2020). The cytokine storm in COVID-19 patients blocks airways, changes vascular permeability and is a cause of exacerbation and even death (Huang et al., 2020a, Xu et al., 2020, Wu et al., 2020). Recent studies on flavonoids showed that flavonoids could be the active ingredients to suppress cytokine release, eliminate inflammation and alleviate the immune response (Wu et al., 2020, Yang et al., 2020, Zhonga et al. 2019). In this study, a flavonoids library consisting of nine different subcategories of flavonoids (consisting of 51 natural flavonoids) was prepared to evaluate in silico interactions and binding affinities against SARS-CoV-2 main Protease and structure–activity relationship (SAR). The physicochemical ADMET (absorption, distribution, metabolism, excretion, and toxicity) properties were also worked out. The kinetic aspects of these compounds have also been worked out. Moreover, the food sources consumed as a preventive measure against SARS-CoV-2 have been figured out from our results.

2. Materials and methods

The docking studies were carried out through Vina (Trott and Olson, 2010) interlinked with MGL tools (Morris et al., 2009). The binding pattern was explored using visualization tools, including Biovia discovery studio (Studio, 2008) and Pymol (DeLano, 2002). The compounds possessing efficient binding affinity were selected for further analysis of absorption, distribution, metabolism, excretion profiling through AdmetSAR (Cheng et al., 2012), http://lmmd.ecust.edu.cn/admetsar2/, a ligand property evaluating tool.

2.1. Preparation of ligands

A ligand library of flavonoids was built (Fig. 1), composed of nine different subcategories of flavonoids. It contains eight prenylated flavonoids (Artonin E, kurarinone, Papyriflavonol
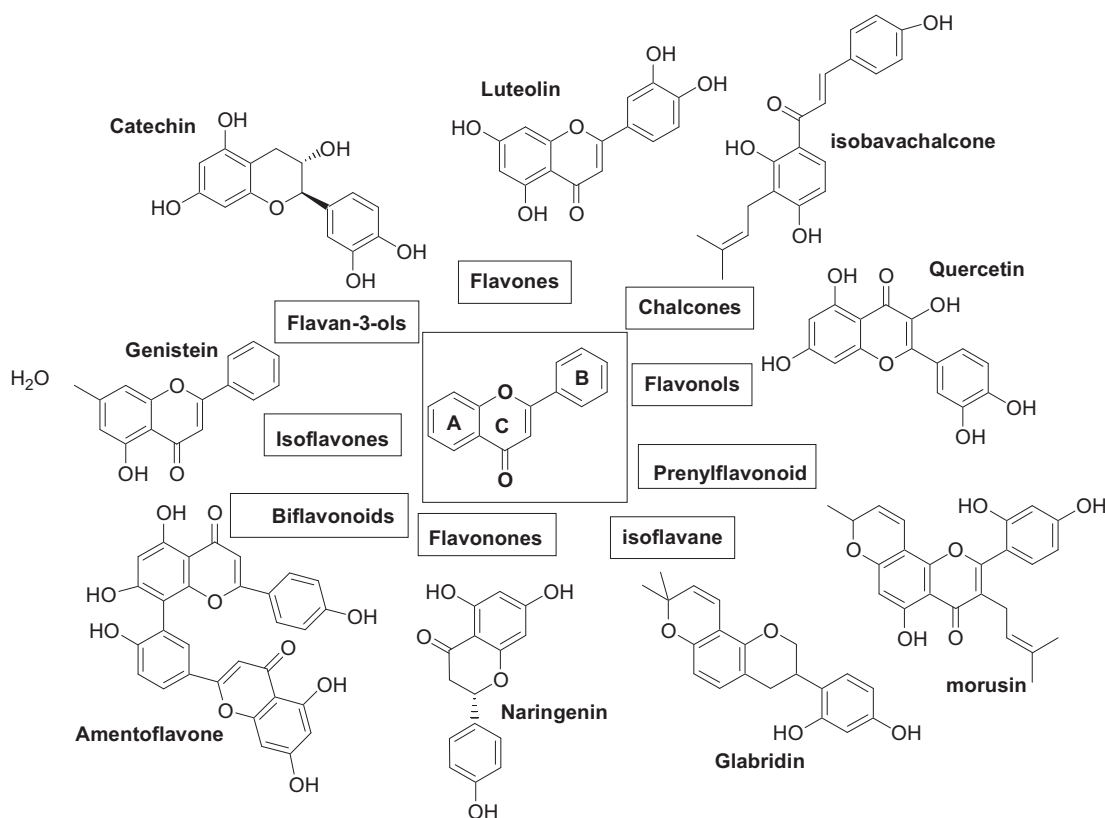
Fig. 1   The basic skeleton of flavonoids and the subcategories used in this study.

A, kuraridin, isoxanthohumol, Kuwanon C, Sophoraflavanone G, morusin), two Biflavonoids (Amentoflavone, Robustaflavone), three chalcones (isobavachalcone, Helichrysetin, Chalconaringenin), two flavan-3-ols (Catechin, Epicatechin), seven Isoflavones and their sugar derivative (Daidzein, Biochanin, Genistein, Daidzin, Genistin, Glycitein, Neobavaisoflavone), one Isoflavane (Glabridin), sixteen Flavone (Chrysin, Baicalein, apigenin, Vitexin, Saponarin, Luteolin, Diosmetin, Tricin, Tangeretin, Gossypetin, Nobiletin, Sinensetin, Wogonin, Oroxylin A, Scutellarein, Cirsilol), six Flavonones (Naringenin, Taxifolin, Dihydrokaempferide, Naringin, Eriodictoyl, Hesperitin) and six flavonols (Quercetin, Kaempferol, Myricetin, Fisetin, Morin, Galangin).

The ligands three-dimensional structures were obtained from the PubChem database (National centre for biochemistry Information, U.S. National Library of Medicine) https://pubchem.ncbi.nlm.nih.gov/ in .sdf format, and structures were drawn on Marvin sketch (https://chemaxon.com/products/marvin) after the literature survey. The molecular energy optimization of ligands was performed using UCSF Chimera (Pettersen et al., 2004). AutoDock tools (ADT1.5.6) [28] were used to set the number of torsions for the flavonoids and COVID-19 3CL^pro/Mpro, and vina files were prepared and saved in pdbqt format.

2.2. Protein preparation

The crystal structure of COVID-19 3CL^pro/Mpro complexed with inhibitor N3 (PDB ID: 6lu7) was downloaded from the protein data bank and used as a target in the screening of selected flavonoids. In preparing the receptor co-crystallized ligands, chain B and water molecules were excluded, and Gasteiger charges were added for a protein using UCSF chimera (Pettersen et al., 2004). The grid size was set to $60 \times 60 \times 60$ x.y.z points having grid spacing of 0.375 Å , and grid recenter (x, y, z): −9.732, 12.695, 69.958, respectively was designated. The NCBI conserved domain (https://www.ncbi.nlm.nih.gov/Structure/cdd/wrpsb.cgi database was used to showed the conserved residues of main protease structure. Aminoacids that are present in the vicinity of 6.5 Å from the N3 inhibitor are considered as main binding residues. The residues such as Thr24, His41, Cys44, Phe140, Thr26, Gly123, His164, Leu27, Glu166, His 172, Leu141, Thr190, Asn142, Gln189 and Gln192 are present in the catalytic pocket of main protease (Fig. 2).

2.3. Molecular docking

Molecular docking studies between the retrieved compounds and main protease were carried out by using AutoDock Vina interlinked with AutoDock MGL tools. The binding pocket of the receptor was well selected using the grid box generation process of AutoDock MGL tools. All the optimized flavonoids are then subjected to docking process, to evaluate their binding pose and binding energy in the active site of main protease. The flavonoids with best conformations and binding affinity with main protease are evaluated by intermolecular interactions.
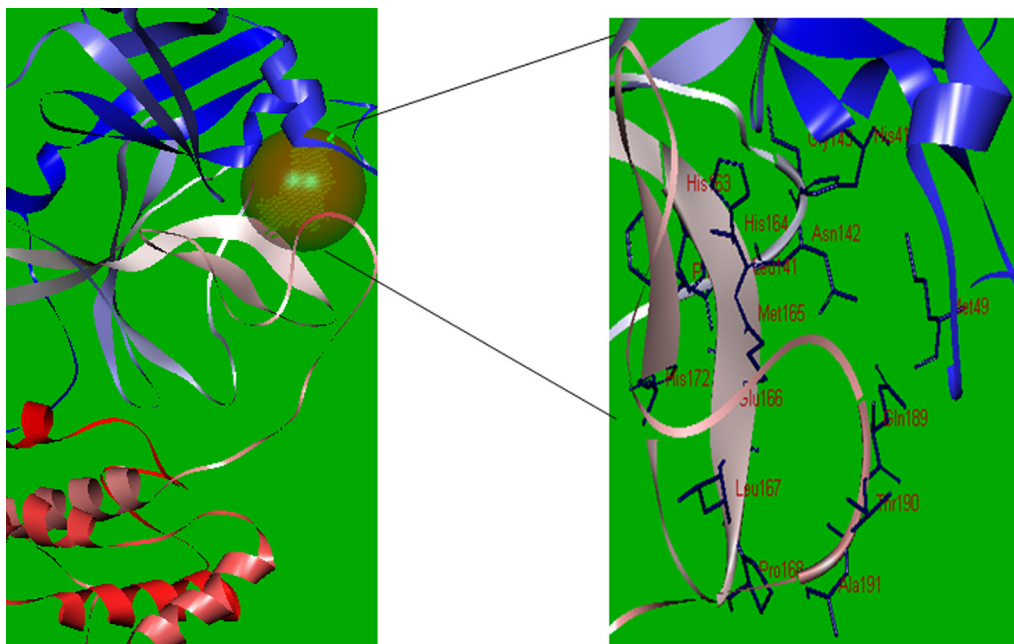
Fig. 2 Structure of main protease of SARS-CoV-2 (PDB ID: 6LU7).

2.4. Molecular dynamic simulation

The compounds with best docking score (i.e. Amentoflavone and Morusin) were further used for molecular dynamic simulation studies. Molecular dynamic was performed for Amentoflavone-M^{pro} complex and Morusin-M^{pro} complex using Desmond module of Schrodinger suite. The complexes were simulated for 100 ns of timescale for understanding the interaction pattern and dynamic behavior (Guo et al., 2010). The prepared complexes were solvated using orthorhombic solvent box conditioned for 10 Å buffer region (Jorgensen et al., 1983). The system in each case was neutralized by adding desired number of counter ions, and the total system consisted of 39,326 atoms and 7697 water molecules. An ensemble (NPT) of Nose-Hoover thermostat used to maintain the constant temperature of 300 K and Martyna-Tobias-Klein barostat was applied to maintain the pressure (Martyna et al., 1992). 1000 steps of steepest descent energy minimization followed by conjugate gradient algorithms were utilized. Smooth particle mesh Ewald method was used to evaluate the short range interactions with cut-off radius of 9 Å and long range coulombic interactions were estimated. Reference system propagator algorithms (RESPA) integration was used in the dynamic study of non-bonded interactions. Trajectories were documented for every 100pc, and the obtained results was analyzed with Maestro graphical interphase.

3. Results and discussion

3.1. Catalytic domain of main protease

NCBI CD results showed that catalytic dyad of M^{pro} composed of two residues like His41 and Cys145, present at the cleft of two domains (domain I and II). Main protease comprises three domains, domain I (amino acid 8–101), domain II (102–184) and domain III (201–303) presented in Fig. 3.

3.2. Molecular properties of selected flavonoids

The flavonoids in nine different scaffolds having the lowest binding energies and highest bonding interactions in the main Protease's catalytic pocket are presented in Table 1. Moreover, Lipinski's rule of five (RO5) and Veber's rule have been employed to determine the drug-likeness and oral activity of compounds under study, respectively. (Lipinski et al., 1997, Lipinski, Giménez et al., 2010, Lipinski, 2004a, 2004b).

It has been found that twelve flavonoids show no violation of RO5 and represent the drug-like molecular nature. Their log P values are within the range of −0.79 to 4.54. Molecular weight, hydrogen bond donor, and hydrogen bond acceptor are within the accepted range except for Amentoflavone and Naringin, which showed two and three violations. Amentoflavone showed a violation of molecular weight and the number of hydrogen bond donors, while Naringin showed a violation of molecular weight, the number of hydrogen bonds, and the acceptor. All the selected flavonoids except Amentoflavone fulfilled the criteria of Veber's rule (Veber et al., 2002) with the number of rotatable bonds and TPSA (total polar surface area) within the range for oral bioavailability. The number of rotatable bonds for drug-like candidates should be less than seven to improve oral bioavailability (Veber et al., 2002). A polar surface area equal to or less than 140 Å is essential for good oral bioavailability. Oral bioavailability is the fractional extent of administered drug that finally reach the site of action (Benet et al., 1996, Kim et al., 2014)

3.3. ADME profiling

The flavonoid's pharmacokinetic properties of all the compounds were calculated using SwissADME (http://www.swissadme.ch/) as shown in Table 2. All flavonoids showed good gastrointestinal absorption, with the probability of the absorption of 96 to 98%. The low absorption rate of the molecules is
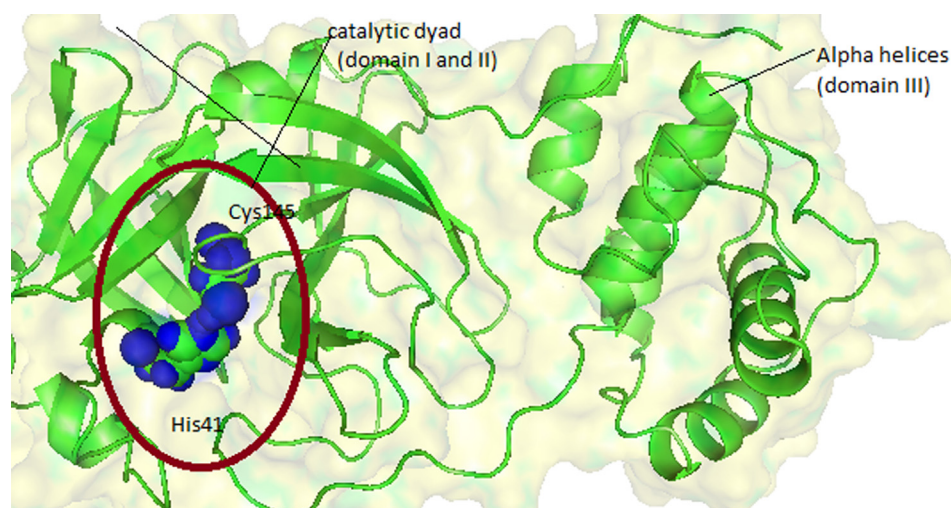
Fig. 3 3D structure of SARS-CoV-2 main protease. Catalytic dyad comprises two residues His41 and Cys145 presented as blue spheres.

Table 1 Molecular properties of selected flavonoids.

Name	AffinityKcal/mol	Lipinski's rule of five				Veber's Rule			
		Molecular weight g/mol	Hydrogen bond donor	Hydrogen bond acceptor	Log p	Violations	Roatatable bonds	tPSA A°2	Heavyatom
Amentoflavone	−9.9	538.46 g/mol	6	10	3.62	2	3	181.80	40
Kaempferol	−8.0	286.24	4	6	1.58	0	1	111.13	21
Baicalein	−8.0	270.24 g/mol	3	5	2.24	0	1	90.90	20
Catechin	−7.6	290.27	5	6	0.85	0	1	110.38	21
Naringin	−8.2	580.53 g/mol	8	14	−0.79	3	6	225.06	41
Naringenin	−7.7	272.25 g/mol	3	5	1.84	0	1	86.99	20
Galangin	−7.8	270.24 g/mol	3	5	1.99	0	1	90.90	20
Kuwanon C	−8.1	422.47 g/mol	4	6	4.54	0	5	111.13	31
Morin	−8.0	302.24 g/mol	5	7	1.20	0	1	131.36	22
Morusin	−8.3	420.45	3	6	4.35	0	3	100.13	31
Scutellarein	−8.3	286.24 g/mol	4	6	1.81	0	1	111.13	21
Wogonin	−8.2	284.26 g/mol	2	5	2.54	0	2	79.90	21
Apigenin	−8.3	270.24 g/mol	3	5	2.11	0	1	90.90	20
Fiestin	−8.0	286.24 g/mol	4	6	1.55	0	1	111.13	21

correlated with their high molecular weight. However, despite its high molecular weight, the Amentoflavone showed an increased absorption of 97%. The solubility range lies between −1 and −5 (Tsaioun and Kates, 2011), and the aqueous solubility of the flavonoids ranges from −3.78 to −2.77 presented moderate to high solubility. The high solubility of flavonoids is due to hydroxy groups that participate in hydrogen bonding with water molecules. The blood–brain barrier is a semipermeable border present within endothelial cells. It prevents the passage of pathogens and large or hydrophilic molecules into the extracellular fluid of the CNS (central nervous system) passage of small polar and hydrophobic molecules (Obermeier et al., 2016). BBB (blood–brain barrier) is the layer of endothelial cells that prevents the entry or exit of solutes from blood stream to the extracellular space. It may be easily evaluated by considering the compound's concentration in the brain's concentration in blood (Obermeier et al., 2016). In the central nervous system, active drugs and high penetrations of the blood–brain barrier are necessary. In contrast, in non-central nervous system active drugs, low penetration reduces the

CNS side effects. The selected flavonoids are not good blood–brain barrier permeant.Table 3

ADMET properties of a useful drug-like compound accepted the following parameters: such as i) absorb the $CaCO_3$ permeability ii) non-toxic iii) non-carcinogenic iv) it must absorb in the human intestine (HI) it must pass the Blood-brain barrier. In the cytochrome p450 inhibitory activity, almost all the selected flavonoids are an inhibitor of CYP to show the drug-drug interactions. CytochromeP450 (CYP) is a family of an enzyme involved in the metabolism of polyunsaturated fatty acids, metabolism of endogenous and exogenous chemicals, and metabolism of toxic compounds, including drugs bilirubin (Berka et al., 2011, Waxman et al., 1991). The apigenin, wogonin, and morusin show the high human colonic adenocarcinoma cell line Caco-2 permeability than other selected compounds. In the case of acute oral Toxicity Apegenin, wogonin, and morusin fall into class III (classification given by the Center for Drug Evaluation and Research) labeled as slightly toxic (Osterberg and See, 2003, Onawole et al., 2018). All the selected flavonoids

Table 2 ADMET properties of potential Flavonoids.

Absorption

	Amentoflavone	Fiestin	Morin 1	Apegenin	Scutellarin	Wogonin	Morusin
Blood-Brain Barrier	BBB+ 0.66	BBB+ 0.51	BBB+ 0.62	BBB+	BBB- 0.57	BBB- 0.63	BBB- 0.64
Human Intestinal Absorption	HIA+ 0.97	HIA+ 0.98	HIA+ 0.98	HIA+ 0.98	HIA+ 0.96	HIA+ 0.97	HIA+ 0.98
Caco-2 Permeability cm/s	Caco2- 0.70	Caco2- 0.40	Caco2- 0.79	Caco2+ 0.89	Caco2- 0.22	Caco2+ 0.91	Caco2+ 1.25
Solubility LogS	−3.36	−3.08	−3.14	−2.77	−2.99	−3.22	−3.78
P-glycoprotein Substrate	Substrate	Substrate	Substrate		Substrate	Substrate	Substrate
Metabolism							
CYP450 1A2 Inhibitor	Inhibitor	Inhibitor	Inhibitor	Inhibitor	Inhibitor	Inhibitor	Inhibitor
CYP450 2C9 Inhibitor	Inhibitor	Inhibitor	Inhibitor	Inhibitor	Non-Inhibitor	Inhibitor	Inhibitor
CYP450 3A4 Inhibitor	Inhibitor	Non– Inhibitor	Inhibitor	Inhibitor	Inhibitor	Inhibitor	Non– Inhibitor
CYP450 2C9 Substrate	Non-substrate	Non-substrate	Non-substrate	Non-substrate	Non-substrate	Non-substrate	Non-substrate
Excretion							
Biodegradation	Not ready biodegradable	Not ready biodegradable	Not ready biodegradable	Not ready biodegradable	Not ready biodegradable	Not ready biodegradable	Not ready biodegradable
Toxicity							
AMES Toxicity	Non AMES Toxic	Non AMES Toxic	Non AMES Toxic	Non AMES Toxic	Non AMES Toxic	Non AMES Toxic	Non AMES Toxic
Carcinogens	Non-carcinogens	Non-carcinogens	Non-carcinogens	Non-carcinogens	Non-carcinogens	Non-carcinogens	Non-carcinogens
Acute oral Toxicity	II 0.62	II 0.71	II 0.62	III 0.70	II 0.73	III 0.73	III 0.70

**Table 3** Bioactivity prediction of selected flavonoids

	$Ki\mu M$	LE	LE_{scale}	LELP	B.E Kcal/mol	FQ
Amentoflavone	0.05	0.24	0.244	15.0	−9.9	0.9
Kaempferol	1.4	0.38	0.44	4.15	−8.0	0.8
Baicalein	1.4	0.4	0.45	5.6	−8.0	0.8
catechin	2.7	0.36	0.44	2.36	−7.6	0.8
Naringin	1	0.2	0.23	−3.95	−8.2	0.8
Naringenin	2.3	0.38	0.45	4.84	−7.7	0.8
galangin	1.9	0.39	0.45	5.1	−7.8	0.8
Kuwanon C	1.9	0.26	0.32	17.46	−8.1	0.8
morin	1.4	0.36	0.42	3.3	−8.0	0.8
morusin	0.8	0.26	0.32	16.7	−8.3	0.8
Scutellarein	0.8	0.39	0.44	4.64	−8.3	0.8
Wogonin	1	0.39	0.44	6.5	−8.2	0.8
Apigenin	0.8	0.41	0.45	5.1	−8.3	0.9
Fiestin	1.4	0.38	0.44	4.07	−8.0	0.8

are predicted to be not readily biodegradable, but all are non-carcinogenic. All the chosen flavonoids showed no AMES toxicity.

3.4. Structure-activity relationships

The structure–activity relationship of flavonoids is derived from the interactions with the main protease active site. The flavonoids of different categories have similar molecular weight values, several rotatable bonds, total polar surface area, and hence activity can be related to hydrogen bond acceptor and donor hydroxyl groups are essential in demonstrating the SARs of flavonoids, especially at positions 3 of ring C, 3′ of ring B, and 7 of ring A (Fig. 4). Herein, we applied a library of flavonoids composed of nine different subcategories.

Apegenin, wogonin and scutellarein, cirsilol, tangeritin, baiclain belongs to subclass flavones having the binding energies of −8.3, −8.2, −8.3, −7.4 and −6.4, −8.1 Kcal/mol, respectively. The lower the binding affinities of scutellarein, apegenin, baiclain, and wogonin with higher interactions were due to hydroxyl group at carbon seven. Scutellarein, baiclain, apegenin, and wogonin have four, three, three, and two hydroxyl groups, respectively. These groups participate in forming a conventional hydrogen bond with active residues (Thr24, His41, Cys44, Phe140, Thr26, Gly123, His164, Leu27, Glu166, His172, Leu141, Thr190, Asn142, Gln189, and Gln192). Hydrogen bonds have an essential role in stability
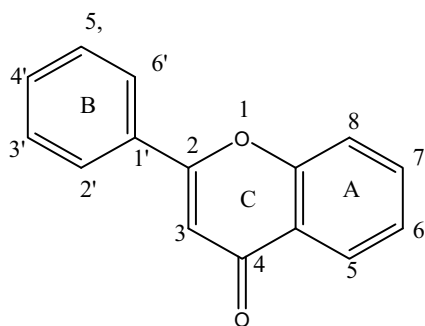
and macromolecular recognition (Klaholz and Moras, 2002). Hydrogen bonds also play a crucial role in several biological processes; hence, hydrogen bonds have a primary role in determining pharmacological receptors. The presence of bulky methyl groups in tangeritin and cirsilol reduces the interactions and increases the binding energy. The binding modes of some representative compounds are presented in Fig. 5. The binding pose of baiclain in the active site of the main protease and 3D interactions are shown in Fig. 6.

According to docking results of prenylated flavonoids, the binding energies of kuwanon C, morusin, Artonin E were −8.1, −8.3 and −9.0 Kcal/mol. Their lower binding energies and higher efficient *in silico* are demonstrated due to the presence of five types of interactions. These interactions are the conventional hydrogen bond, pi-donor hydrogen bond, pi-sigma, pi-alkyl and alkyl type. Although Kuwanon C formed the five conventional hydrogen bonds with active residues, the binding energy of Artonin E was much lower than Kuwanon C. It may be due to the presence of other types of interaction that stabilized the ligand-receptor complex. Moreover, from docking results it was cleared that hydrophobic substituent may enhanced the bioactivity of the compounds. The binding pattern of prenylated flavonoids is represented in Fig. 7.

Naringenin, Eriodictoyl, kaempferide, Hesperetin belong to the subcategory flavanones. The binding energy of no one compound was less than −8.0Kcal/mol, although they have a hydroxyl group at position seven. The binding affinity of Eriodictoyl was −7.4Kcal/mol, and it formed the conventional bonds with critical residues. Naringenin formed the six conventional hydrogen bonds with Thr190, Glu166, His163, and Leu141, having the binding affinity of −7.7 Kcal/mol. Naringin is a disaccharide derivative of naringenin that presented the binding affinity of −8.2Kcal/mol. It means that sugar residue by substituting hydroxyl group resulted in a decrease in binding energy with higher interactions. The binding modes of Hesperetin, Naringenin are depicted in Fig. 8. In bioflavonoids, namely Amentoflavone, robustaflavone presented the lowest binding affinity in the whole library of flavonoids. The binding affinity of **Amentoflavone** (Bioflavonoids) was **−9.9 kcal/mol**. It showed six types of interactions (Van der Waals, conventional hydrogen bond, pi-donor hydrogen bond,
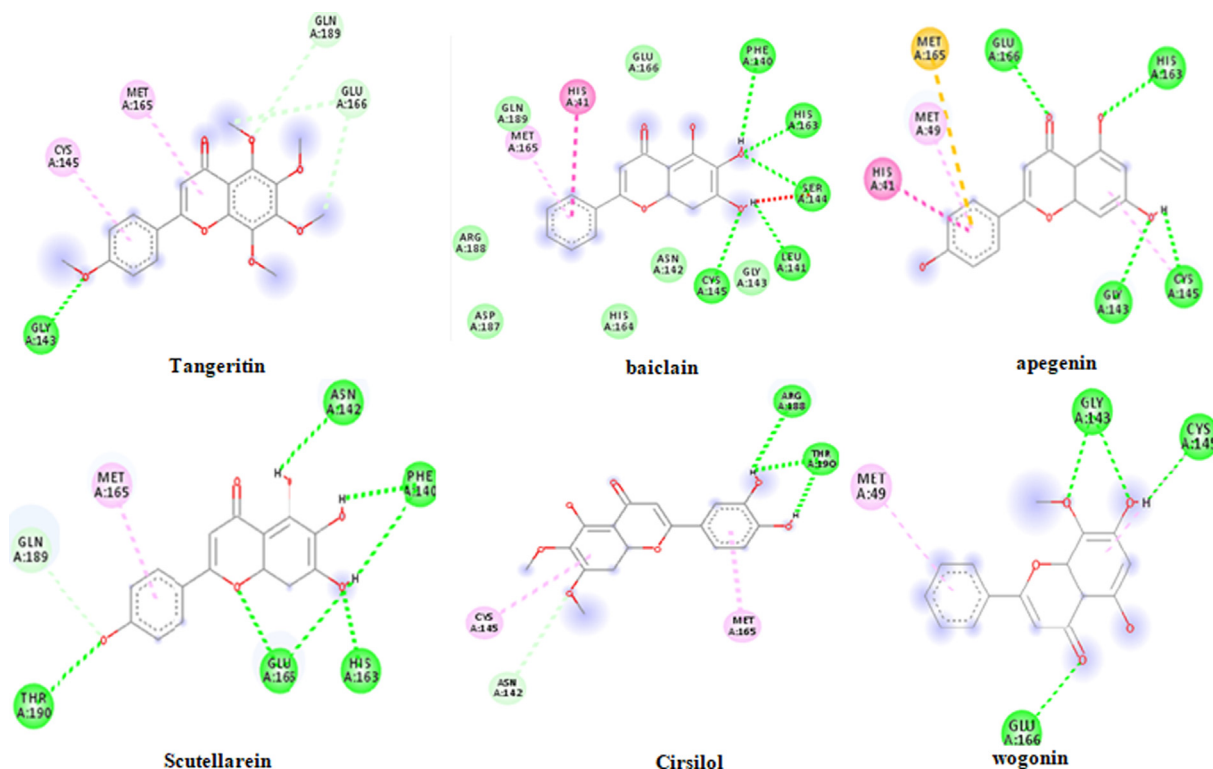

Fig. 4 General structure and numbering pattern of flavonoids.

Fig. 5 The molecular interactions of Tangeritin, baiclain, apegenin, Scutellarein, Cirsilol and wogonin with amino residues in 6LU7.
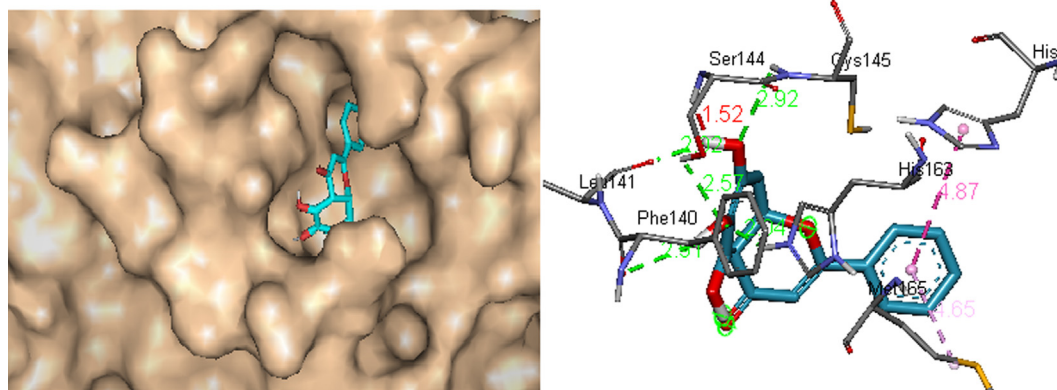

Fig. 6 The binding pose of baiclain in the active site of SARS-CoV-2 main Protease.

pi-sulfur, pi-pi T-shaped, and pi-Alkyl). Two conventional hydrogen bonds formed by His163 and Thr26 were shown as green dotted lines, and one was pi-sulfur interaction shown by Cys145 with benzopyran ring of **Amentoflavone**. The **Amentoflavone** showed one of the pi-donor hydrogen bond interaction type with Glu166, a pi-alkyl type with Leu141, Met165, and a pi-pi T-shaped interaction with His41. Hydrophobic contact formed by the Gln189, Arg188, Asp187, Tyr54, Met49, His164, His172, Phe140, Ser144, Leu141, Gly143, Leu27, Thr25, Thr26, and Asn142 that ligand-receptor complex illustrated in Fig. 8 and the Fig. 9 showed the binding pose of **Amentoflavone** in the pocket of SARS-Cov-2 main Protease. Amentoflavone showed the higher bioactivity than the parent compound (apegenin). While the robustaflavone showed the interactions with residues of domain III of 6LU7.

Among the studied flavonoids, flavonols like Morin, Fisetin, Quercetin have binding energies of −8.0, −8.0, and −7.2 Kcal/mol. Morin showed four types of interaction, including conventional hydrogen bond, pi-sulfur, pi-alkyl, and pi-sigma. **Morin** formed six conventional hydrogen bonds with Tyr54, Cys145, Leu141, Gln189, and Glu166 residues of the pocket. **Morin** showed the pi-sulfur interaction, pi-alkyl, and pi-sigma with Met165, Met49, and His41. The **Fisetin** (Flavonol) inhibitor showed three types of interactions with M^{pro} of COVID-19, four hydrogen bonds with His41 (2.87 Å), His163 (2.20 Å), Leu141 (2.01 Å), and Phe140 (1.86 Å) and pi-alkyl interactions with Met165, Met49, Cys145. **Fisetin** also has strong hydrophobic contact with Asp187, Gly143, Asn142, Ser144, His172, Glu166, His164, Gln189 Arg18 8. The predicted 2D interaction was depicted in Fig. 10. The docking
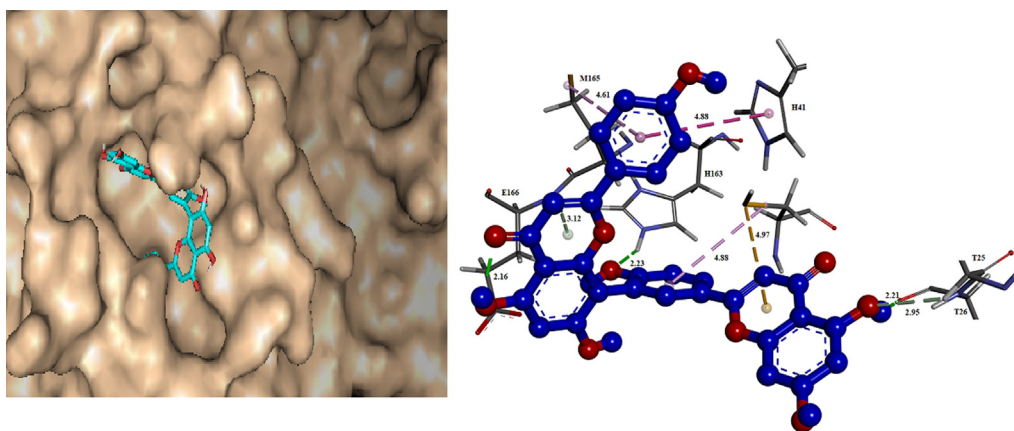
Fig. 7 The molecular interactions of Artonin E, Kuwanon C, Morusin, Hesperetin, Naringenin and Morin with amino residues in 6LU7.

Fig. 8 The molecular SAR interactions of Daidezin, Chalconaringenin, Fiestin, Amentoflavone, and Catechin with amino residues in 6LU7.

Fig. 9 The binding pose of Amentoflavone in the active site of SARS-CoV-2 main Protease.
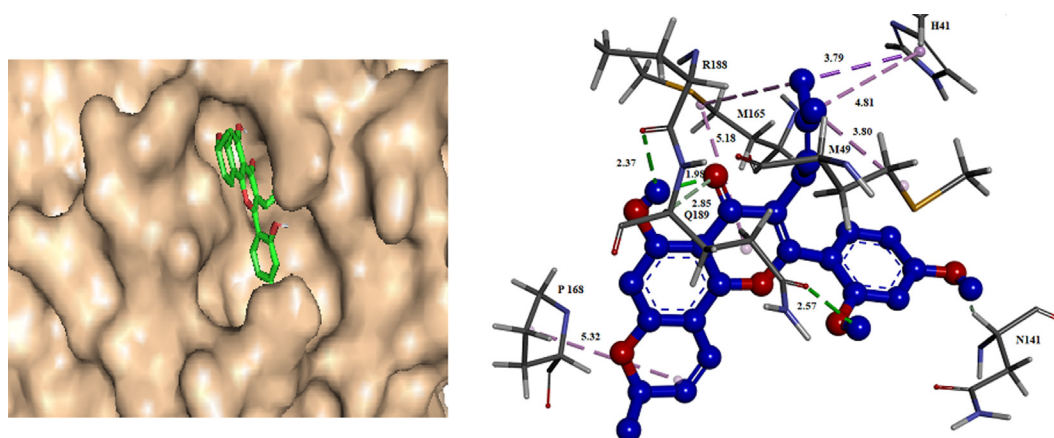
Fig. 10 The binding pose and 3D interactions of Morusin in the active site of SARS-CoV-2 main Protease.

results of isoflavones showed that Daidzein's two hydroxyl groups formed the four hydrogen bonds with Arg188, Leu141, Cys145 and Gly143 with the binding affinity of −7.5Kcal/mol Fig. 10. In Chalcones and Flavan-3-ols, the lower binding energy (-7.1Kcal/mol) was observed in Chalconaringenin has four free hydroxyl groups that formed hydrogen bonds with His163, Leu141, Gly143, and Arg188 (Fig. 10). While in Flavan-3-ols the lower binding energy (-7.6Kcal/mol) of Catechin may be due to presence of five free hydroxyl groups and in these four conventional hydrogen bonds was observed with Phe140, Glu166, and Gln189 key residues. The type and amount of bonding exhibited by the inhibitor in the protein's active site showed the compounds' affinity toward the drug. In flavonoids, the number and position of hydroxyl groups are essential in determining the inhibitory potential. In addition to conventional hydrogen bonds, other types of interactions like van der waals, pi-sigma, pi-sulfur, pi-alkyl, and carbon-hydrogen bonds are also important in accelerating the inhibitory potential of flavonoids.

3.5. Bioactivity prediction of best docked flavonoids

The AutoDcok vina score presented in Table1 has been further used to calculate the inhibition constant (Ki) using Eq. (1). The compounds with low inhibition constant values, usually in the micromolar range had a higher likelihood of pharmacological promiscuity (Onawole et al., 2018). All the flavonoids with efficient binding affinity showed the inhibition constant within the micromolar range and qualified as lead compounds. The inhibition constant was calculated using Eq. (1). Other derivable ligand efficiency metrics were estimated using Eqs. (2)–(5). The other metric ligand efficiency (LE) is used to calculate potency's efficiency per heavy atom in a ligand. The threshold value of ligand efficiency and fit quality (FQ) for drug-like candidates should be between 0.3 and 0.8, respectively (Murray et al., 2014, Keserü and Makara, 2009, Leeson and Springthorpe, 2007, Reynolds et al., 2007, Schultes et al., 2010). The ligand efficiency in lipophilicity is known as ligand efficiency lipophilic price, denoted as LELP, is expected to be within the range of −10 to 10. All the selected flavonoids presented in Table 4 except Amentoflavone, Kuwanon C and Morusin have LELP values within the expected range. For fit quality, all the chosen flavonoids have values within the stipulated range.

$$Ki = 10^{[binding\,energy \div 1.366]} \tag{1}$$

$$Ligand\ efficiency(LE) = -B.E \div H.A \tag{2}$$

Table 4 Classification and food sources of some dietary flavonoids

Class	Flavonoids	Dietary source	References
Flavones	luteolin, apigenin, luteolin glycoside	Fruit skin, red wine, red pepper, tomato skin, parsley, capsicum pepper, Chinese cabbage, grapes, bell pepper	(Miean and Mohamed, 2001, Hertog et al., 1992)
Flavonols	Querectin, kaemferol, myricetin, baicalein, Morin	Onion, red wine, olive oils, grape fruits, apples, tomatoes, bell pepper	(Stewart et al., 2000, Dabeek and Marra, 2019)
Flavanones	Hesperitin, naringin, naringenin, hesperidin	Citrus fruits, grape fruits, lemons, oranges	(Rouseff et al., 1987, Salehi et al., 2019, Dr, 2005)
Isoflavone	Genistin, daidzein, glycitein	Soy flour, soy beans, soy milk, beef, fava beans	(Zhang et al., 1999, Thompson et al., 2006)
Flavan-3-ols	Catechin, cianidanol epicatechin,	Green tea, beans cherry, chocolate,	(Egert and Rimbach, 2011)
Anthocyanins	Cyanidin, apigenidin	Cherry, strawberry,	(Kumar and Pandey, 2013)
Biflavonoids	Amentoflavone, Robustaflavone	Japanese tallow or wax tree	(Khan and Khan, 2020)
Prenylated flavonoids	Morusin, kuwanon C	Barks of Morus nigra	(ABD EL-MAWLA et al., 2011)

$$LE_{scale} = 0.873e^{-0.026 \times H.A.} - 0.064 \qquad (3)$$

$$FQ = LE \div LE_{scale} \qquad (4)$$

$$Ligand - efficiency - dependent\ lipophilicity(LELP)$$
$$= LogP \div LE \qquad (5)$$

3.6. MD simulation

The 100 ns MD simulations of M^{pro} complexed with Amentoflavone and Morusin were performed using Desmond. The fluctuation and stability of the receptor-ligand complexes during simulations in each case was analyzed and resulting trajectory was made with backbone root mean square deviation.
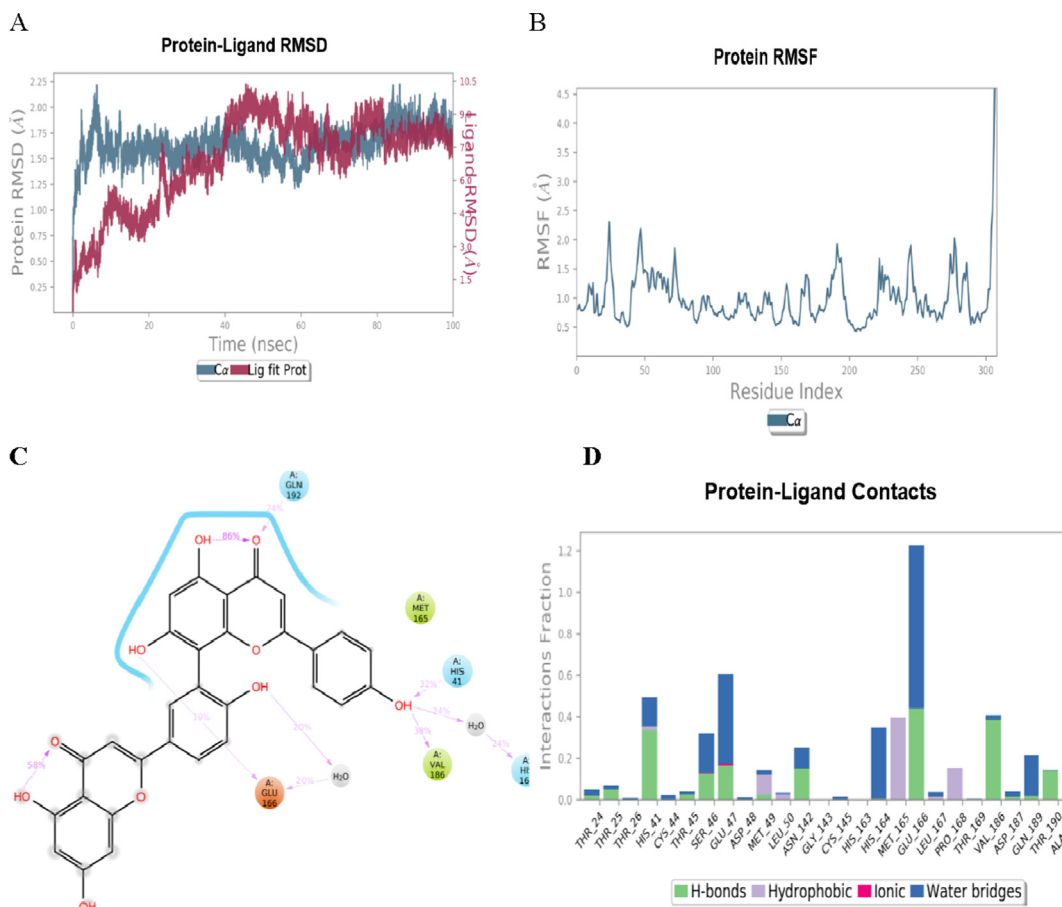

Fig. 11 Molecular dynamics trajectory analysis of Amentoflavone (A) RMSD of the protein and ligand with respect to the first frame (B) Protein RMSF (C)) Ligand-protein contacts (D) Protein-ligand contacts histogram.
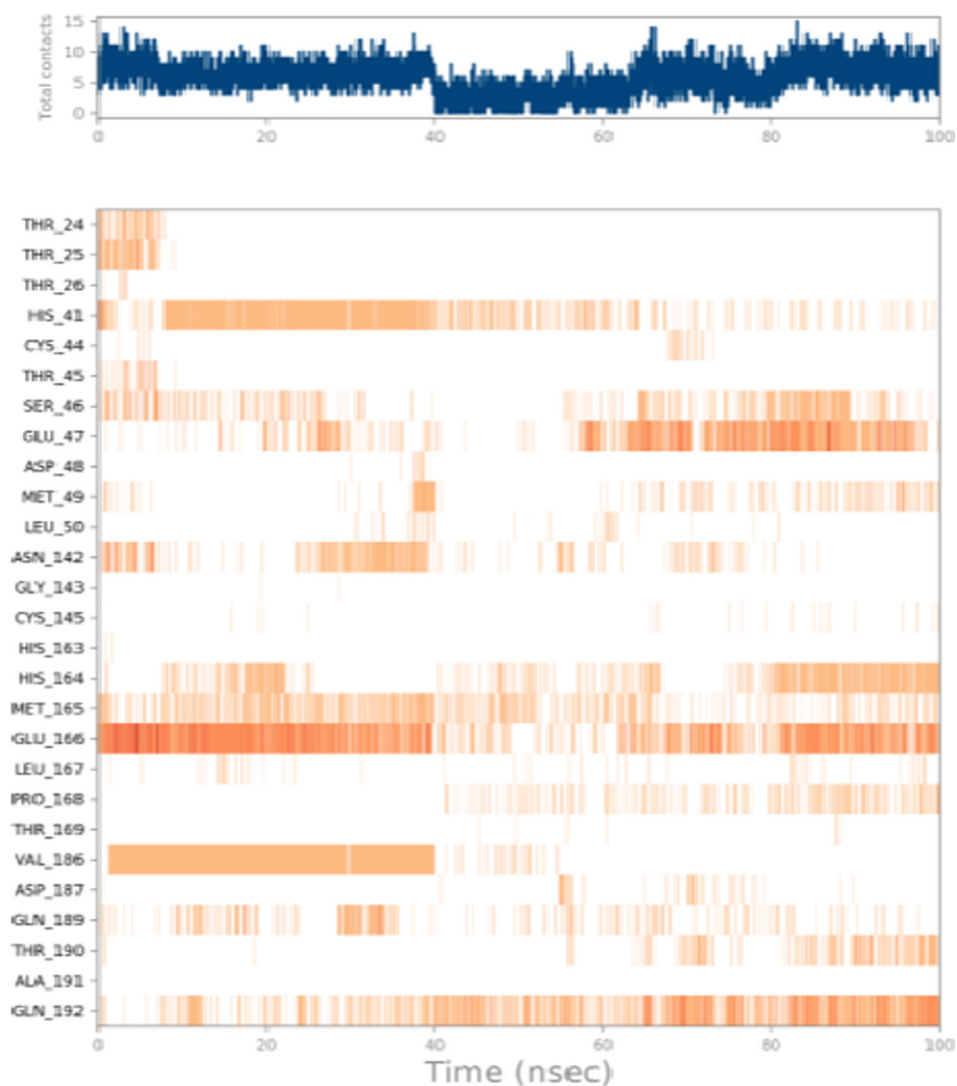
Fig. 12 Timeline representation of the interaction and contacts, top panel show specific contact of amentoflavone and protein during 100 ns simulation.

It was observed that overall protein ligand was stable during entire simulation. Some fluctuations in protein were observed for first 10 ns then it remained stable for next 90 ns. Some ligand fluctuations were observed that might be due to hydrogen bond formation (Fig. 11A). Root mean square fluctuation (RMSF) was studied to recognize the major fluctuations in the domain of protein. Peaks in the plot indicated that the major fluctuation in the loop region of protein was observed after 300 residues. This might be due to that alpha helices and beta strands were more rigid than unstructured (loop region) of the protein (Fig. 11B). A total of 27 ligand contacts were observed with residues of protein, from Thr24 to Leu50, Asn142 to Cys145, His163 to Thr169 and Val186 to Gln192. These residues formed four types of interactions including Hydrogen Bonds, Hydrophobic, Ionic and Water Bridges. It was observed that ligand achieved stability by forming polar and hydrophobic interaction with the active residues (Fig. 11D). The schematic details of ligand atoms two dimensional interactions with protein residues is presented in Fig. 11 C. It showed the actual percentage of interactions

between ligand and protein. In this case, residues such as Glu166 (20%), Val186 (38%) and His41 (32%) formed the hydrogen bond during most of the time of simulation. Different types of contacts such as H bond, hydrophobic, ionic and water bridges between protein and ligand during simulation were observed and presented in Fig. 12. Top panel indicated the total contacts that M^{pro} makes with the amentoflavone over the course of the trajectory whereas specific residues level interaction with the ligands in each trajectory frame are shown in bottom panel. In addition to that, multiple specific contacts with amentoflavone were formed with some residues which are represented by dark orange shade. Furthermore in first 40 ns Glu166 formed the hydrogen bond along with other type of interactions. Fig. 13 presents the MD trajectory analysis data for the morusin-Mpro complex. Ligand-protein complex remained almost stable throughout the simulation and the RMSD value ranged from 0.8 to 3.0 Å for both morusin and main protease complex (Fig. 13A). The flexibility of protein was also checked by evaluating the Root mean square fluctuations (RMSF) of individual residues of main protease. The
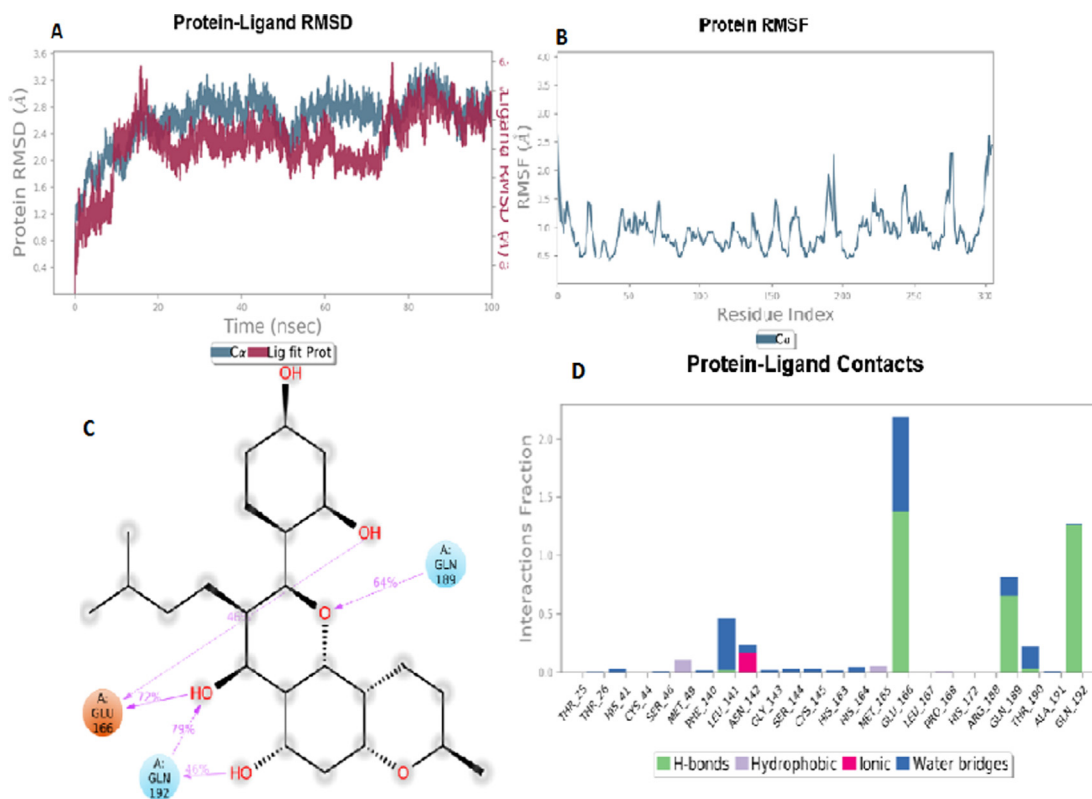
Fig. 13 Molecular dynamics trajectory analysis of Morusin (A) RMSD of the protein and ligand with respect to the first frame (B) Protein RMSF (C)) Ligand-protein contacts (D) Protein-ligand contacts histogram.

entire main protease had an RMSF value between 0.5 and 1.5 Å except for the terminal amino acid residues this might be due to that N and C terminal move rapidly than any other part of the protein (Fig. 13B). The interaction between morusin and active residues of main protease is depicted in Fig. 13C and it presented the actual percentage of interaction. It was observed that Glu166 (72% and 46%), Gln189 (64%) and Gln192 (79% and 46%) interact through hydrogen bonding. The Fig. 13D showed the fraction analysis of morusin with main protease during 100 ns simulation period. The major active residues were found to interact through hydrogen bonding and water bridges with ligand. Finally, a timeline of the morusin-main protease interactions is plotted in the form of hydrogen-bonds, hydrophobic contact, ionic interaction and water bridges during 100 ns of simulation period. The top panel presents the total contacts of morusin-main protease complex and the bottom panel indicates residue level interaction of the morusin. Overall, the morusin interacted well with the main protease binding pocket, especially, Glu166 Gln192 showed the efficient contact with ligand throughout the simulation period (Fig. 14).

3.7. Comparison of inhibitors of M^pro or 3CL pro with experimental results

The experimental results recently reported for some of the flavonoids against M^pro have been presented in Table 5 which supported our findings through molecular docking and MD simulation studies. The experimental data also showed that bioactivity of the compounds against SARS MPro depended on the modifications in their molecular structures. Amentoflavone, a biflavone in proved to be more potent than apegenin (parent compound). The compounds with substituted groups exerted stronger inhibition than parent compound. Moreover prenylated flavonoids (Morusin, Kuwanon C) having the hydrophobic substituent were presented in literature with good inhibitory potential against influenza virus. Generally the prenylation of flavonoids generally enhanced the bioactivity and bioavailability of the compounds (Grienke et al., 2016).

3.8. Food sources of some common flavonoids

The food sources for some common dietary flavonoids belonging to nine different subcategories are presented in Table 4. These dietary sources are rich in flavonoids contents and may be used without any special precautions or trials for the prevention from the risk of COVID-19.

4. Conclusion

The present study aims to identify the inhibitory activity of various flavonoids against SARS-CoV-2 M^pro. This study discovered the strong bonding interactions of flavonoids (Amentoflavone, scutellarin, moursin, apigenin, wogonin, kaempferol, fiestin, kaempferol, kuwanon C and morin with catalytic site of main Protease. The study also concluded that bioflavonoids, prenylated flavonoids, Flavones, Flavanones, and Flavan-3-ols showed better interaction and binding affinity in the active site of main Protease. At the same time, Isofla-

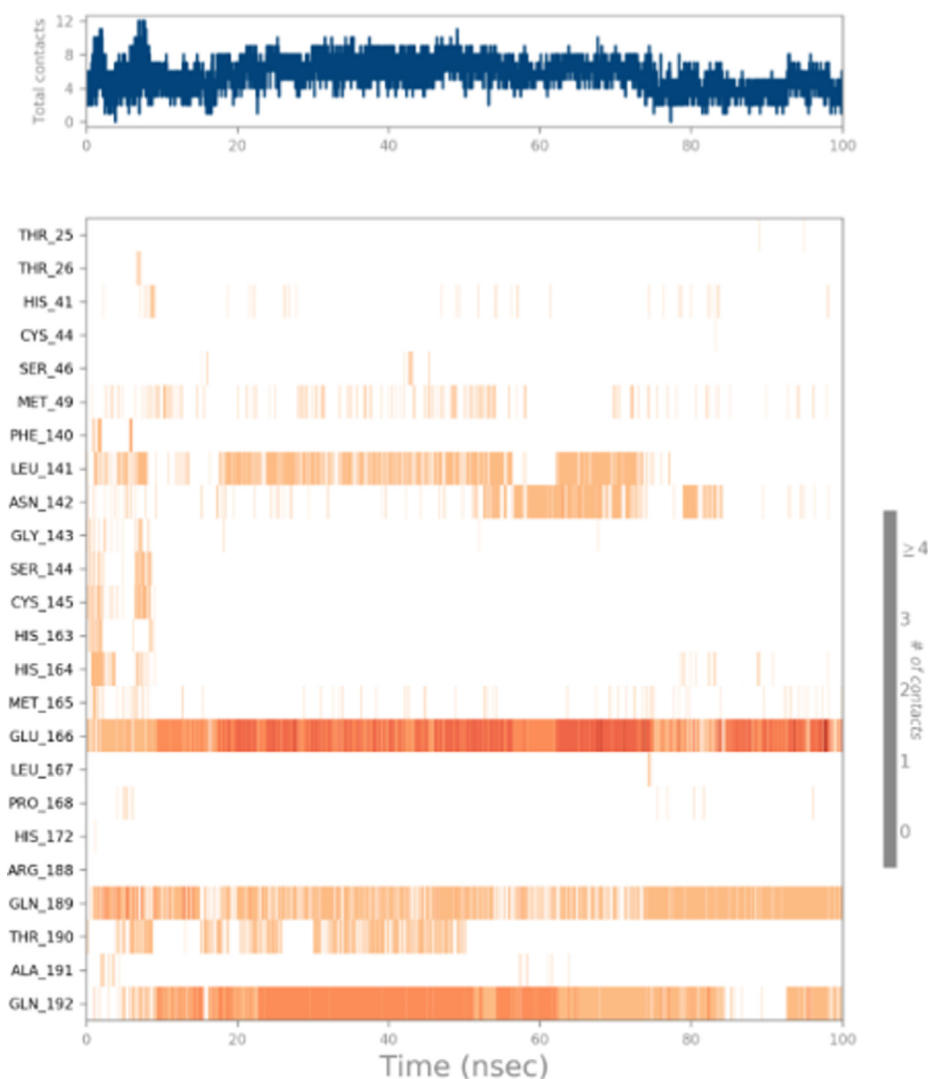## Protein-Ligand Contacts (cont.)

Fig. 14 Timeline representation of the interaction and contacts, top panel show specific contact of morusin and main protease during 100 ns simulation.

Table 5 Comparison of theoretical findings to experimentally reported data

	Substance	B.E Kcal/mol	SARS 3CLpro or Mpro IC50 μM
Flavonole	Ksaempferol	−8.0	116.3 (Jo et al., 2020)
Flavones	Amentoflavone	−9.9	8.3 (Jo et al., 2020)
	Apegenin	−8.3	280 (Jo et al., 2020)
	Scutellarein	−8.3	0.86 against nsp13 (Keum and Jeong, 2012)

vone and isoflavone have not presented the prominent binding affinities. Moreover, the strong binding affinity of flavones (especially amentoflavone and morusin) with M^{pro} was further supported/strengthened by the results achieved from molecular dynamic simulation, where the complexes of ligands with main protease remained stable over a time of 100 ns. The flavonoids with the lowest binding energies were analyzed for their pharmacokinetic properties. These studies revealed that these flavonoids from medicinal plants could be used as strong drug candidates against the main Protease of SARS CoV-2. In light of the above results, we further conclude that flavonoids may serve as future drug candidates against SARS CoV-2 and encourage the in vivo and in vitro investigation of these compounds. Moreover, the use of food sources listed in Table 4 may serve as an essential preventive measure against SARS CoV-2 and helpful in adjuvant therapy of SARS CoV-2 patients.

Data availability

The datasets generated during and/or analyzed during the current study are available from the corresponding author on reasonable request

Code availability

Not applicable.

Author's contributions

S. I. -conducting research and partial analysis of results; A. H. and M. S. - Conceptualization and preparing a manuscript; A. R. A. -planning research, partial analysis of results; J. U. - planning research, analysis results, and preparing a manuscript. M. I. - original draft preparation and analysis: L. M. T. K. and M. K. – methodology, formal analysis, and investigation.

References

Abd El-Mawla, A., Mohamed, K.M., Mostafa, A.M., 2011. Induction of biologically active flavonoids in cell cultures of Morus nigra and testing their hypoglycemic efficacy. Sci. Pharm. 79, 951–962.

Amin, S.A., Banerjee, S., Ghosh, K., Gayen, S., Jha, T., 2020. Protease targeted COVID-19 drug discovery and its challenges: Insight into viral main protease (Mpro) and papain-like protease (PLpro) inhibitors. Bioorg. Med. Chem. 115860.

Anand, K., Palm, G.J., Mesters, J.R., Siddell, S.G., Ziebuhr, J., Hilgenfeld, R., 2002. Structure of coronavirus main proteinase reveals combination of a chymotrypsin fold with an extra α-helical domain. EMBO J. 21, 3213–3224.

Báez-Santos, Y.M., John, S.E.S., Mesecar, A.D., 2015. The SARS-coronavirus papain-like protease: structure, function and inhibition by designed antiviral compounds. Antiviral Res. 115, 21–38.

Benet, L.Z., Kroetz, D., Sheiner, L., Hardman, J., Limbird, L., 1996. Pharmacokinetics: the dynamics of drug absorption, distribution, metabolism, and elimination. Goodman Gilman's the Pharm. Basis Therapeutics 3, e27.

Berka, K., Hendrychová, T., Anzenbacher, P., Otyepka, M., 2011. Membrane position of ibuprofen agrees with suggested access path entrance to cytochrome P450 2C9 active site. J. Phys. Chem. A 115, 11248–11255.

Cheng, F., Li, W., Zhou, Y., Shen, J., Wu, Z., Liu, G., Lee, P.W., Tang, Y., 2012. admetSAR: a comprehensive source and free tool for assessment of chemical ADMET properties. ACS Publications.

Colson, P., Rolain, J.-M., Lagier, J.-C., Brouqui, P., Raoult, D., 2020. Chloroquine and hydroxychloroquine as available weapons to fight COVID-19. Int. J. Antimicrob. Agents 55, 105932.

Dabeek, W.M., Marra, M.V., 2019. Dietary quercetin and kaempferol: Bioavailability and potential cardiovascular-related bioactivity in humans. Nutrients 11, 2288.

Delano, W.L., 2002. Pymol: An open-source molecular graphics tool. CCP4 Newsletter on protein crystallography 40, 82–92.

DR, D. J. 2005. Duke's Phytochemical and Ethnobotanical Databases. Artemisia annua.

Drosten, C., Günther, S., Preiser, W., van der Werf, S., Brodt, H.-R., Becker, S., Rabenau, H., Panning, M., Kolesnikova, L., Fouchier, R.A., 2003. Identification of a novel coronavirus in patients with severe acute respiratory syndrome. N. Engl. J. Med. 348, 1967–1976.

Egert, S., Rimbach, G., 2011. Which sources of flavonoids: complex diets or dietary supplements? Adv. Nutrition 2, 8–14.

Giménez, B., Santos, M., Ferrarini, M., Fernandes, J., 2010. Evaluation of blockbuster drugs under the rule-of-five. Die Pharmazie-An Int. J. Pharm. Sci. 65, 148–152.

Grienke, U., Richter, M., Walther, E., Hoffmann, A., Kirchmair, J., Makarov, V., Nietzsche, S., Schmidtke, M., Rollinger, J.M., 2016. Discovery of prenylated flavonoids with dual activity against influenza virus and Streptococcus pneumoniae. Sci. Rep. 6, 1–11.

Guo, Z., Mohanty, U., Noehre, J., Sawyer, T.K., Sherman, W., Krilov, G., 2010. Probing the α-helical structural stability of stapled p53 peptides: molecular dynamics simulations and analysis. Chem. Biol. Drug Des. 75, 348–359.

Havsteen, B., 1983. Flavonoids, a class of natural products of high pharmacological potency. Biochem. Pharmacol. 32, 1141–1148.

Hertog, M.G., Hollman, P.C., Katan, M.B., 1992. Content of potentially anticarcinogenic flavonoids of 28 vegetables and 9 fruits commonly consumed in the Netherlands. J. Agric. Food. Chem. 40, 2379–2383.

Huang, C., Wang, Y., Li, X., Ren, L., Zhao, J., Hu, Y., Zhang, L., Fan, G., Xu, J., Gu, X., 2020a. Clinical features of patients infected with 2019 novel coronavirus in Wuhan, China. lancet 395, 497–506.

Huang, C., Wang, Y., Li, X., Ren, L., Zhao, J., Hu, Y., Zhang, L., Fan, G., Xu, J., Gu, X. 2020. Wei Y1. Wu W, Xie X, Yin W, Li H, Liu M, Xiao Y, Gao H, Guo L, Xie J, Wang G, Jiang R, Gao Z, Jin Q, Wang J and Cao B, 497-506.

Hui, D.S., Azhar, E.I., Madani, T.A., Ntoumi, F., Kock, R., Dar, O., Ippolito, G., McHugh, T.D., Memish, Z.A., Drosten, C., 2020. The continuing 2019-nCoV epidemic threat of novel coronaviruses to global health—The latest 2019 novel coronavirus outbreak in Wuhan, China. Int. J. Infectious Dis. 91, 264–266.

Imran, M., Irfan, A., Ibrahim, M., Assiri, M.A., Khalid, N., Ullah, S., Al-Sehemi, A.G., 2020. Carbonic anhydrase and cholinesterase inhibitory activities of isolated flavonoids from Oxalis corniculata L. and their first-principles investigations. Ind. Crops Prod. 148, 112285.

Ivashkiv, L.B., Donlin, L.T., 2014. Regulation of type I interferon responses. Nat. Rev. Immunol. 14, 36–49.

Jo, S., Kim, S., Shin, D.H., Kim, M.-S., 2020. Inhibition of SARS-CoV 3CL protease by flavonoids. J. Enzyme Inhib. Med. Chem. 35, 145–151.

Jorgensen, W.L., Chandrasekhar, J., Madura, J.D., Impey, R.W., Klein, M.L., 1983. Comparison of simple potential functions for simulating liquid water. J. Chem. Phys. 79, 926–935.

Keserü, G.M., Makara, G.M., 2009. The influence of lead discovery strategies on the properties of drug candidates. Nat. Rev. Drug Discovery 8, 203–212.

Keum, Y.-S., Jeong, Y.-J., 2012. Development of chemical inhibitors of the SARS coronavirus: viral helicase as a potential target. Biochem. Pharmacol. 84, 1351–1358.

Khan, S.A., Khan, B., 2020. Anatomy, micromorphology, and physiochemical analysis of Rhus succedanea var. himalaica root. Microsc. Res. Tech. 83, 424–435.

Kim, M.T., Sedykh, A., Chakravarti, S.K., Saiakhov, R.D., Zhu, H., 2014. Critical evaluation of human oral bioavailability for pharmaceutical drugs by using various cheminformatics approaches. Pharm. Res. 31, 1002–1014.

Klaholz, B.P., Moras, D., 2002. C-H··· O Hydrogen Bonds in the Nuclear Receptor RARγ—a Potential Tool for Drug Selectivity. Structure 10, 1197–1204.

Kumar, S., Pandey, A.K., 2013. Chemistry and biological activities of flavonoids: an overview. Sci. World J., 2013.

Leeson, P.D., Springthorpe, B., 2007. The influence of drug-like concepts on decision-making in medicinal chemistry. Nat. Rev. Drug Discovery 6, 881–890.

Li, G., Fan, Y., Lai, Y., Han, T., Li, Z., Zhou, P., Pan, P., Wang, W., Hu, D., Liu, X., 2020. Coronavirus infections and immune responses. J. Med. Virol. 92, 424–432.

Li, W., Moore, M.J., Vasilieva, N., Sui, J., Wong, S.K., Berne, M.A., Somasundaran, M., Sullivan, J.L., Luzuriaga, K., Greenough, T.

C., . Angiotensin-converting enzyme 2 is a functional receptor for the SARS coronavirus. Nature 426, 450–454.

Lipinski, C. Drug Discovery Today: Technol., 2004, vol. 1, no. 4.

Lipinski, C.A., 2004b. Lead-and drug-like compounds: the rule-of-five revolution. Drug Discovery Today: Technologies 1, 337–341.

Lipinski, C.A., Lombardo, F., Dominy, B.W., Feeney, P.J., 1997. Experimental and computational approaches to estimate solubility and permeability in drug discovery and development settings. Adv. Drug Deliv. Rev. 23, 3–25.

Martyna, G.J., Klein, M.L., Tuckerman, M., 1992. Nosé-Hoover chains: The canonical ensemble via continuous dynamics. J. Chem. Phys. 97, 2635–2643.

Miean, K.H., Mohamed, S., 2001. Flavonoid (myricetin, quercetin, kaempferol, luteolin, and apigenin) content of edible tropical plants. J. Agric. Food. Chem. 49, 3106–3112.

Morris, G.M., Huey, R., Lindstrom, W., Sanner, M.F., Belew, R.K., Goodsell, D.S., Olson, A.J., 2009. AutoDock4 and AutoDockTools4: Automated docking with selective receptor flexibility. J. Comput. Chem. 30, 2785–2791.

Murray, C.W., Erlanson, D.A., Hopkins, A.L., Keserü, G.R.M., Leeson, P.D., Rees, D.C., Reynolds, C.H., Richmond, N.J., 2014. Validity of ligand efficiency metrics. ACS Publications.

Musarrat, F., Chouljenko, V., Dahal, A., Nabi, R., Chouljenko, T., Jois, S.D., Kousoulas, K.G., 2020. The anti-HIV drug nelfinavir mesylate (Viracept) is a potent inhibitor of cell fusion caused by the SARSCoV-2 spike (S) glycoprotein warranting further evaluation as an antiviral against COVID-19 infections. J. Med. Virol. 92, 2087–2095.

Obermeier, B., Verma, A., Ransohoff, R.M., 2016. The blood–brain barrier. Handbook of clinical neurology. Elsevier.

Onawole, A.T., Kolapo, T.U., Sulaiman, K.O., Adegoke, R.O., 2018. Structure based virtual screening of the Ebola virus trimeric glycoprotein using consensus scoring. Comput. Biol. Chem. 72, 170–180.

Osterberg, R.E., See, N.A., 2003. Toxicity of excipients—a food and drug administration perspective. Int. J. Toxicol. 22, 377–380.

Pettersen, E.F., Goddard, T.D., Huang, C.C., Couch, G.S., Greenblatt, D.M., Meng, E.C., Ferrin, T.E., 2004. UCSF Chimera—a visualization system for exploratory research and analysis. J. Comput. Chem. 25, 1605–1612.

Pietta, P.-G., 2000. Flavonoids as antioxidants. J. Nat. Products 63, 1035–1042.

Reynolds, C.H., Bembenek, S.D., Tounge, B.A., 2007. The role of molecular size in ligand efficiency. Bioorg. Med. Chem. Lett. 17, 4258–4261.

Rouseff, R.L., Martin, S.F., Youtsey, C.O., 1987. Quantitative survey of narirutin, naringin, hesperidin, and neohesperidin in citrus. J. Agric. Food. Chem. 35, 1027–1030.

Salehi, B., Fokou, P.V.T., Sharifi-Rad, M., Zucca, P., Pezzani, R., Martins, N., Sharifi-Rad, J., 2019. The therapeutic potential of naringenin: a review of clinical trials. Pharmaceuticals 12, 11.

Schultes, S., de Graaf, C., Haaksma, E.E., de Esch, I.J., Leurs, R., Krämer, O., 2010. Ligand efficiency as a guide in fragment hit selection and optimization. Drug Discovery Today: Technologies 7, e157–e162.

Stewart, A.J., Bozonnet, S., Mullen, W., Jenkins, G.I., Lean, M.E., Crozier, A., 2000. Occurrence of flavonols in tomatoes and tomato-based products. J. Agric. Food. Chem. 48, 2663–2669.

Studio, D., 2008. Discovery Studio. Accelrys [2.1].

Thompson, L.U., Boucher, B.A., Liu, Z., Cotterchio, M., Kreiger, N., 2006. Phytoestrogen content of foods consumed in Canada, including isoflavones, lignans, and coumestan. Nutr. Cancer 54, 184–201.

Trott, O., Olson, A.J., 2010. AutoDock Vina: improving the speed and accuracy of docking with a new scoring function, efficient optimization, and multithreading. J. Comput. Chem. 31, 455–461.

Tsaioun, K., Kates, S.A., 2011. ADMET for medicinal chemists: a practical guide. John Wiley & Sons.

Tufan, A., Güler, A.A., Matucci-Cerinic, M., 2020. COVID-19, immune system response, hyperinflammation and repurposing antirheumatic drugs. Turkish J. Med. Sci. 50, 620–632.

Veber, D.F., Johnson, S.R., Cheng, H.-Y., Smith, B.R., Ward, K.W., Kopple, K.D., 2002. Molecular properties that influence the oral bioavailability of drug candidates. J. Med. Chem. 45, 2615–2623.

Walls, A.C., Park, Y.-J., Tortorici, M.A., Wall, A., McGuire, A.T., Veesler, D., 2020. Structure, function, and antigenicity of the SARS-CoV-2 spike glycoprotein. Cell.

Waxman, D.J., Lapenson, D.P., Aoyama, T., Gelboin, H.V., Gonzalez, F.J., Korzekwa, K., 1991. Steroid hormone hydroxylase specificities of eleven cDNA-expressed human cytochrome P450s. Arch. Biochem. Biophys. 290, 160–166.

Wu, H., Wang, J., Yang, Y., Li, T., Cao, Y., Qu, Y., Jin, Y., Zhang, C., Sun, Y., 2020. Preliminary exploration of the mechanism of Qingfei Paidu decoction agains novel coronavirus pneumonia based on network pharmacology and molecular docking technology. Acta Pharmaceutica Sinica. DO I, 10.

Xu, Z., Shi, L., Wang, Y., Zhang, J., Huang, L., Zhang, C., Liu, S., Zhao, P., Liu, H., Zhu, L., 2020. Pathological findings of COVID-19 associated with acute respiratory distress syndrome. Lancet Respiratory Med. 8, 420–422.

Yamamoto, N., Yang, R., Yoshinaka, Y., Amari, S., Nakano, T., Cinatl, J., Rabenau, H., Doerr, H.W., Hunsmann, G., Otaka, A., 2004. HIV protease inhibitor nelfinavir inhibits replication of SARS-associated coronavirus. Biochem. Biophys. Res. Commun. 318, 719–725.

Yang, R., Liu, H., Bai, C., Wang, Y., Zhang, X., Guo, R., Wu, S., Wang, J., Leung, E., Chang, H., 2020. Chemical composition and pharmacological mechanism of Qingfei Paidu Decoction and Ma Xing Shi Gan Decoction against Coronavirus Disease 2019 (COVID-19): in silico and experimental study. Pharmacol. Res. 104820.

Zaki, A.M., van Boheemen, S., Bestebroer, T.M., Osterhaus, A.D., Fouchier, R.A., 2012. Isolation of a novel coronavirus from a man with pneumonia in Saudi Arabia. N. Engl. J. Med. 367, 1814–1820.

Zhang, H., Penninger, J.M., Li, Y., Zhong, N., Slutsky, A.S., 2020. Angiotensin-converting enzyme 2 (ACE2) as a SARS-CoV-2 receptor: molecular mechanisms and potential therapeutic target. Intensive Care Med. 46, 586–590.

Zhang, Y., Wang, G.-J., Song, T.T., Murphy, P.A., Hendrich, S., 1999. Urinary disposition of the soybean isoflavones daidzein, genistein and glycitein differs among humans with moderate fecal isoflavone degradation activity. J. Nutrition 129, 957–962.

Zhong, N., Zheng, B., Li, Y., Poon, L., Xie, Z., Chan, K., Li, P., Tan, S., Chang, Q., Xie, J., 2003. Epidemiology and cause of severe acute respiratory syndrome (SARS) in Guangdong, People's Republic of China, in February, 2003. Lancet 362, 1353–1358.

Zhonga, L.L.D., Lama, WC, Yanga, W., Chanb, K.W., Cho, S., Szec, W., Miaod, J., Yungc, K.K.L., Biana, Z., Taam, V. Potential Targets for Treatment of Coronavirus Disease 2019 (COVID-19): A Review of Qing-Fei-Pai-Du-Tang and its Major Herbs.

Ziebuhr, J., Snijder, E.J., Gorbalenya, A.E., 2000. Virus-encoded proteinases and proteolytic processing in the Nidovirales. J. Gen. Virol. 81, 853–879.